Journal of Medicinal Chemistry

Article

Cite This: J. Med. Chem. 2018, 61, 8174−8185

pubs.acs.org/jmc

Stabilized β-Hairpin Peptide Inhibits Insulin Degrading Enzyme

Dan Yang,[†,‡,#] Weirong Qin,[†,#] Xiaodong Shi,[†] Bili Zhu,[§] Mingsheng Xie,[†] Hui Zhao,[†] Bin Teng,[∥,⊥] Yujie Wu,[†] Rongtong Zhao,[†] Feng Yin,[†] Peigen Ren,[∥,⊥] Lizhong Liu,[§] and Zigang Li*[,†]

[†]State Key Laboratory of Chemical Oncogenomics, School of Chemical Biology & Biotechnology, Peking University Shenzhen Graduate School, Shenzhen 518055, Guangdong, China

[‡]Department of Science & Technology of Shandong Province, Jinan 250101, Shandong, China

[§]School of Medicine, Shenzhen University, Shenzhen 518055, Guangdong, China

[∥]Center for Translational Medicine Research and Development, Shenzhen Institutes of Advanced Technology, Chinese Academy of Sciences, Shenzhen 518055, Guangdong, China

[⊥]Shenzhen College of Advanced Technology, University of Chinese Academy of Sciences, Shenzhen 518055, Guangdong, China

Supporting Information

ABSTRACT: Insulin-degrading enzyme (IDE) plays a critical role in both the proteolytic degradation and inactivation of insulin. The exploration of novel IDE inhibitors could aid in the study of novel therapeutics for type-2 diabetes. Herein, we report a hypothesized stabilized β-hairpin peptide that can efficiently inhibit the enzymatic activity of IDE. The resulting stabilized peptide **B35** is demonstrated to activate the AKT phosphorylation pathway in skeletal muscle cells and is shown to slow insulin degradation. An 80 mg kg^{-1} intraperitoneal (i.p.) injection of the stabilized β-hairpin peptide **B35** is demonstrated to improve glucose tolerance during an oral glucose tolerance test in obese mouse model. We note that this stabilized peptide exhibited negligible cytotoxicity in both *in vitro* and *in vivo* assays, even at high concentrations (300 μM). This study suggests that IDE peptide inhibitors could function as potentially meaningful candidates for the development of type-2 diabetes therapeutics.

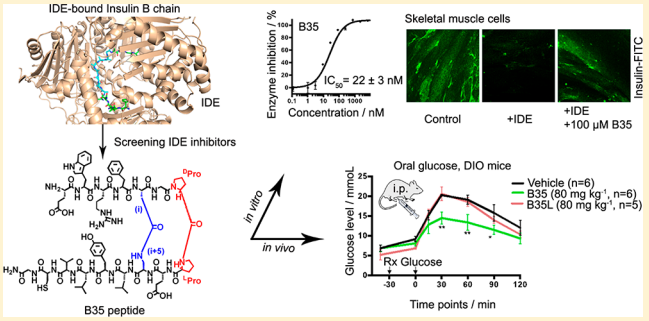

INTRODUCTION

Insulin is one of the most well studied peptide hormones and remains to be one of the most critical therapeutics used for type-2 diabetes since its first application in the early 1920s.[1] Insulin-degrading enzyme (IDE) is a 113 kDa secreted zinc−metalloprotease and plays critical roles in the proteolytic degradation and inactivation of insulin and other peptides,[2−4] including glucagon and amyloid β.[5−7] IDE is a member of the metallopeptidase superfamily M16 and possesses two catalytic domains at its N- and C-terminal,[8,9] respectively, which are connected via a flexible linker. This structural feature enables IDE to switch between an "open" and "closed" state.[10] The open state allows substrate entry and access to the catalytic zinc site. After substrate entry, the IDE−substrate complex adopts the closed state, and the bound substrate is subsequently degraded. IDE is found primarily in the cytosol and peroxisomes[11,12] and is thought to be a potential therapeutic target for the treatment of type-2 diabetes mellitus (T2DM) and Alzheimer's disease.[13−17] However, the relationship between IDE and glucose homeostasis remains largely elusive.

An inactivating mutation in the IDE gene has been demonstrated to cause failed insulin secretion in the Goto−Kakizaki (GK) rat model of T2DM. In 2007, a genome wide association study identified novel risk loci for T2DM and demonstrated that IDE is a diabetes susceptibility gene.[18] Loss of IDE function has been implicated in pancreatic β cell failure, as the Ide$^{-/-}$ mouse exhibits impaired insulin secretion.[19]

Evidence suggests that IDE inhibitors could improve glucose tolerance under conditions that mimic meal intake. Recent studies have identified novel IDE inhibitors by using a DNA-templated library or a proteomic analysis of cleavage sites.[13,20,21] Saghatelian and Liu et al. reported a cyclic-peptide inhibitor **6bk** (Figure 1A) from a DNA-templated macrocycle library screening.[21] Inhibitor **6bk** recognizes a binding pocket located away from the catalytic site, shows antidiabetic activity, and causes a substantially improved oral glucose tolerance in both lean and diet-induced obese (DIO) mouse model.

Peptides, like insulin and glucagon-like peptide-1(GLP-1) analogues, are attractive candidates for the treatment of type-2 diabetes.[22−24] However, peptides are generally rapidly degraded by peptidases *in vivo*.[25,26] Methods including amino acid mutation and side chain/backbone modification are

Received: March 14, 2018
Published: August 27, 2018

DOI: 10.1021/acs.jmedchem.8b00418
J. Med. Chem. 2018, 61, 8174−8185

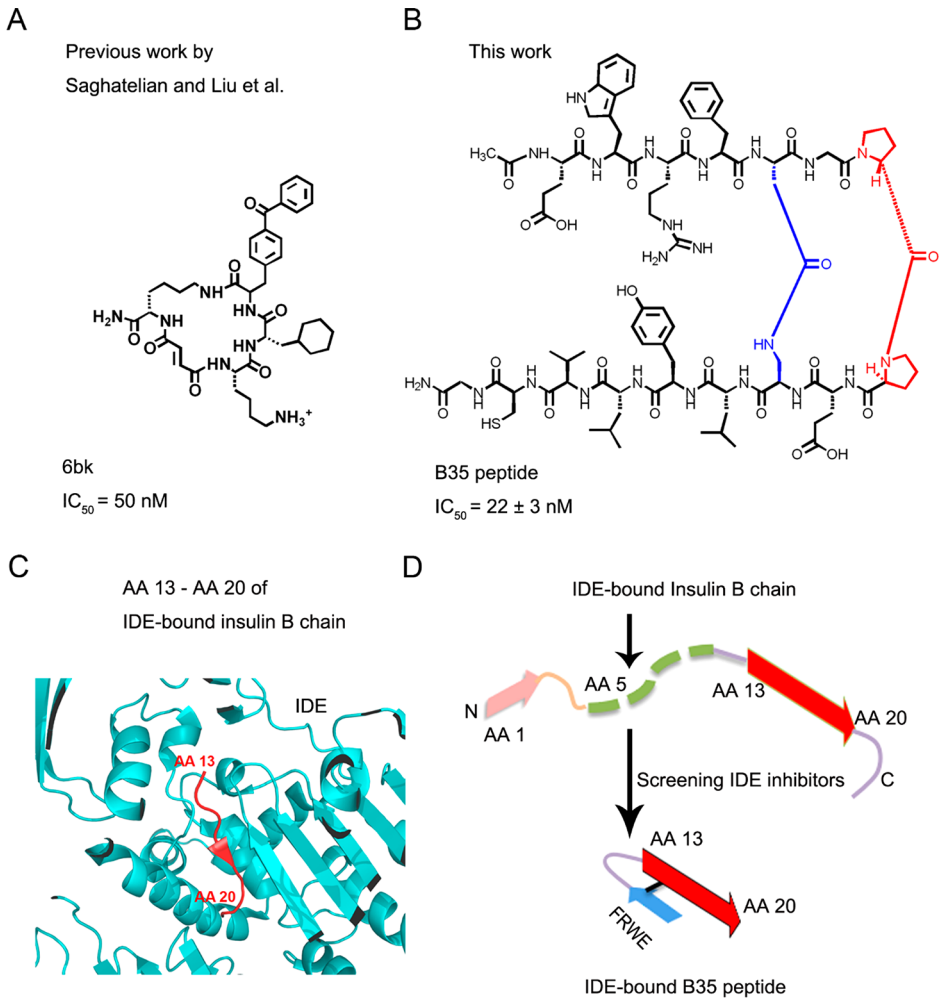

Figure 1. (A) Previously reported IDE inhibitor, **6bk** (IC_{50} = 50 nM in protease assays). (B) Amino acid sequence of peptide **B35** (IC_{50} = 22 ± 3 nM in protease assays). (C) Secondary structure representation of AA 13−AA 20 (red) of the IDE-E111Q-insulin B chain complex (PDB: 2G56).[9] (D) Schematic presentation of the proposed binding pattern of insulin B chain and **B35** with IDE.

utilized to retain peptide activity while enhancing stability and cell permeability.[27−32] For example, Gellman et al. utilized the substitution of α-amino acid residues with β amino acid residues to make GLP-1-derived oligopeptides with engendering prolonged activity *in vivo*.[33,34]

These pioneering studies have intrigued us to work toward the development of suitable stabilized peptide-based inhibitors against IDE enzymes. Numerous chemical strategies have been developed to constrain peptides into helical and β-sheet/β-hairpin structures.[27,35−39] In the case of β-hairpin stabilization, turn mimetic, including ^{D}Pro-^{L}Pro,[40,41] ^{D}Pro-Gly,[42−44] Aib-Gly,[45] azobenzenes,[46] and dibenzofuran derivatives,[47,48] are broadly utilized to induce the initial β-hairpin formation. Due to the flexible nature of β-sheets in solution, macrocyclizations via disulfide bridges, thiol-ether, and/or amide bond formation at precise positions are commonly used to enable additional stabilization effects for longer peptide sequences.[49]

By studying the structure of the IDE-E111Q-insulin B chain complex, we noted that the N-terminal five amino acids and the cleavage-site-containing eight amino acids from insulin B exist as β-sheets and interact with IDE strands β12 and β6, respectively (Figure 1C). We hypothesized that a stabilized β-hairpin peptide that mimics the insulin B chain binding sequence EALYLVCG could function as a suitable and stable IDE inhibitor. A ^{D}Pro-^{L}Pro turn inducer was plotted for the initial β-hairpin nucleation, and a further macrocyclization was proposed to generate additional stabilization. Following rational design, screening, and evolution of a panel of peptides, we now report an efficient hypothesized β-hairpin peptide IDE inhibitor, **B35** (Figure 1B). Peptide **B35** showed a satisfying binding affinity with IDE (K_D = 22 ± 5 nM), an efficient inhibition of IDE enzymatic activity (IC_{50} = 22 ± 3 nM), and potentiated insulin signaling at the cellular level. The intraperitoneal (i.p.) injection of peptide **B35** (80 mg kg^{-1}) resulted in improved glucose tolerance in the DIO mouse models. Peptide **B35** was evolved from natural existing sequences and exhibited negligible cytotoxicity in both *in vitro* and *in vivo* studies. Our work further supports the idea that pharmacological inhibition of IDE could serve as an attractive approach for the treatment of diabetes, and suggests that stabilized peptides could be of potential applications.

RESULTS AND DISCUSSION

Based on the reported fluorogenic peptide substrate Mca-RPPGFSAFK(Dnp)−OH,[13,21] we used protease assays to test the efficiency of IDE inhibiting peptides. With the original IDE binding sequence EALYLVCG, peptide **B1** did not exhibit good enzyme inhibition activity (Table 1; Supporting

DOI: 10.1021/acs.jmedchem.8b00418
J. Med. Chem. 2018, 61, 8174−8185

Table 1. IC_{50} Value of Peptides Determined by Protease Assays Using the Reported Fluorophore/Quencher-Tagged Peptide Substrate Mca-RPPGFSAFK(Dnp)−OH[a]

Peptide	Sequence	IC_{50} (nM)
B1	H-EALYLVCG-NH_2	230 ± 20
B14	H-EWRF^{D}P^{L}PEALYLVCG-NH_2	74 ± 5
B21	H-EWRF^{D}P^{L}PEALYLV-NH_2	86 ± 2
B22	H-RF^{D}P^{L}PEALYLV-NH_2	>20000
B23	H-EWRF^{D}P^{L}PEALY-NH_2	601 ± 29
B24	H-RF^{D}P^{L}PEALY-NH_2	>20000
B30	H-EALYLVCG^{D}P^{L}PFRWE-NH_2	170 ± 13
B33	H-EWRFGGEALYLVCG-NH_2	300 ± 40
B35	H-EWRF-cyclo(DG^{D}P^{L}PEDap)LYLVCG-NH_2	22 ± 3
B36	H-EWRF-cyclo(DGGG^{D}P^{L}PEDap)LYLVCG-NH_2	44 ±13
B37	H-EWRF-CG^{D}P^{L}PEC-LYLVCG-NH_2 (thioether)	60 ± 5
B38	H-EWRF-CGGG^{D}P^{L}PEC-LYLVCG-NH_2 (thioether)	77 ± 30
B35L	H-EFLWAG^{D}P^{L}PYACVGRLE-NH_2	n.d.
Bacitracin	---	>200000

[a]Abbreviations: IC_{50}, half maximal inhibitory concentration of peptides in protease assays; n.d., not determined.

Information, Figure S1). We then utilized the ^{D}Pro-^{L}Pro template in order to induce a rigid type-II β-turn. In previous reports, Phe-Arg-Trp-Glu[13,20] was identified as IDE ligands with limited activity from proteomic analyses of IDE cleavage sites with a combinatorial mixture of short peptides. Taking advantages of knowing IDE ligand Phe-Arg-Trp-Glu and insulin B chain segment, we further designed a series of β-hairpin peptides. Following necessary screening, peptide **B14** was found to exhibit an intriguing IDE inhibitory activity with a half-maximum inhibitory concentration of 74 nM (Table 1). The sequences were then truncated from both the C- and the N-terminus to produce peptide **B21−24**. All truncations showed detrimental effects on IDE inhibition. Based on our results, the N-terminus amino acids, Trp and Glu, are indispensable for IDE inhibition.

Based on the side chain to side chain cross-linking method published previously,[50,51] we began from 2,3-diaminopropionic acid (Dap) and aspartic acid to introduce an amide bond between the two side chains of **B14** (Scheme 1). Designed cyclic peptidomimetics hold great promise for the structural and functional mimicry of protein surfaces, and cyclization may enhance the peptide's serum stability and cellular uptakes.[52−54] We hypothesized that this amide bond bridge could help to fine-tune the peptides' secondary structure into a more stable β-hairpin. Thioether dipeptide linkers were also tested (**B37**, **B38**; Scheme1 and Table 1). Finally, we found peptide **B35** (Figure 1B,D, Scheme1, and Table 1) with the lowest IC_{50} of approximately 22 nM (Table 1 and Figure 2A). In *in vitro* protease assays, **B35** peptide showed ≥1000-fold selectivity for inhibition of IDE over other metalloproteases tested (angiotensin-converting enzyme (ACE), endothelin-converting enzyme-1 (ECE-1), and neprilysin (NEP)) (Figure 2A).

In order to evaluate the binding affinity of the stabilized peptides with IDE, we generated and purified the catalytically inactive IDE mutant, IDE-E111Q (primer sequences were shown in Table S1). Peptide **B35** labeled with N-terminal FITC was found to have high affinity with IDE-E111Q (K_D = 22 ± 5 nM, Figure 2B). According to circular dichroism (CD) spectra, **B35** and **B14** were found to exhibit typical β-haripin

Scheme 1. Flowchart of the Evolution of IDE Inhibitors Using the Strategy of Amido Linkage Cyclization or Thioether-Cyclization[a]

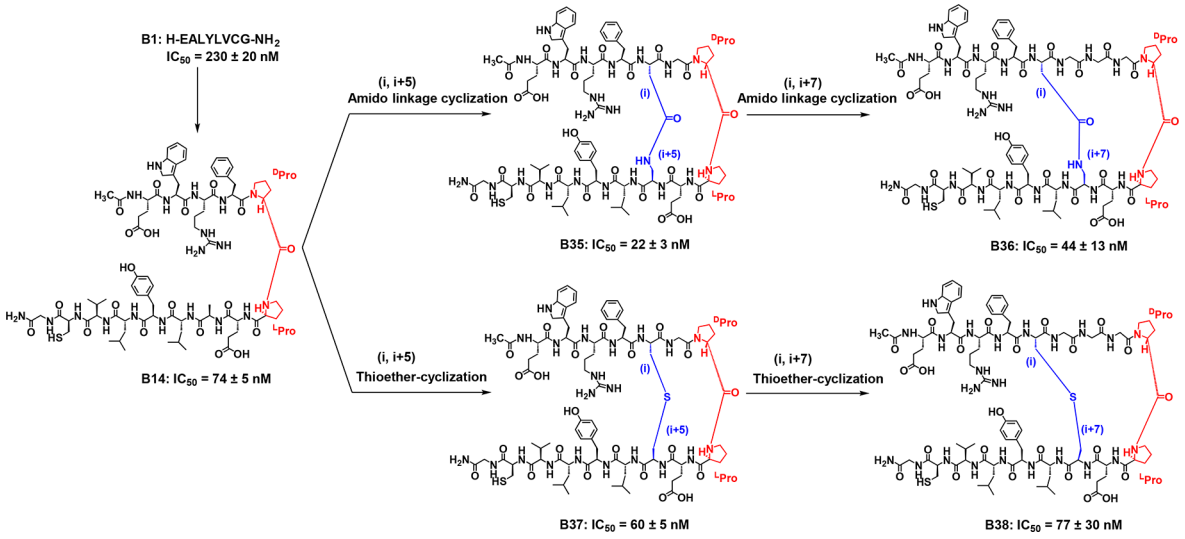

[a]IC_{50} value of enzyme inhibition activity with protease assays is given under each structure.

DOI: 10.1021/acs.jmedchem.8b00418
J. Med. Chem. 2018, 61, 8174−8185

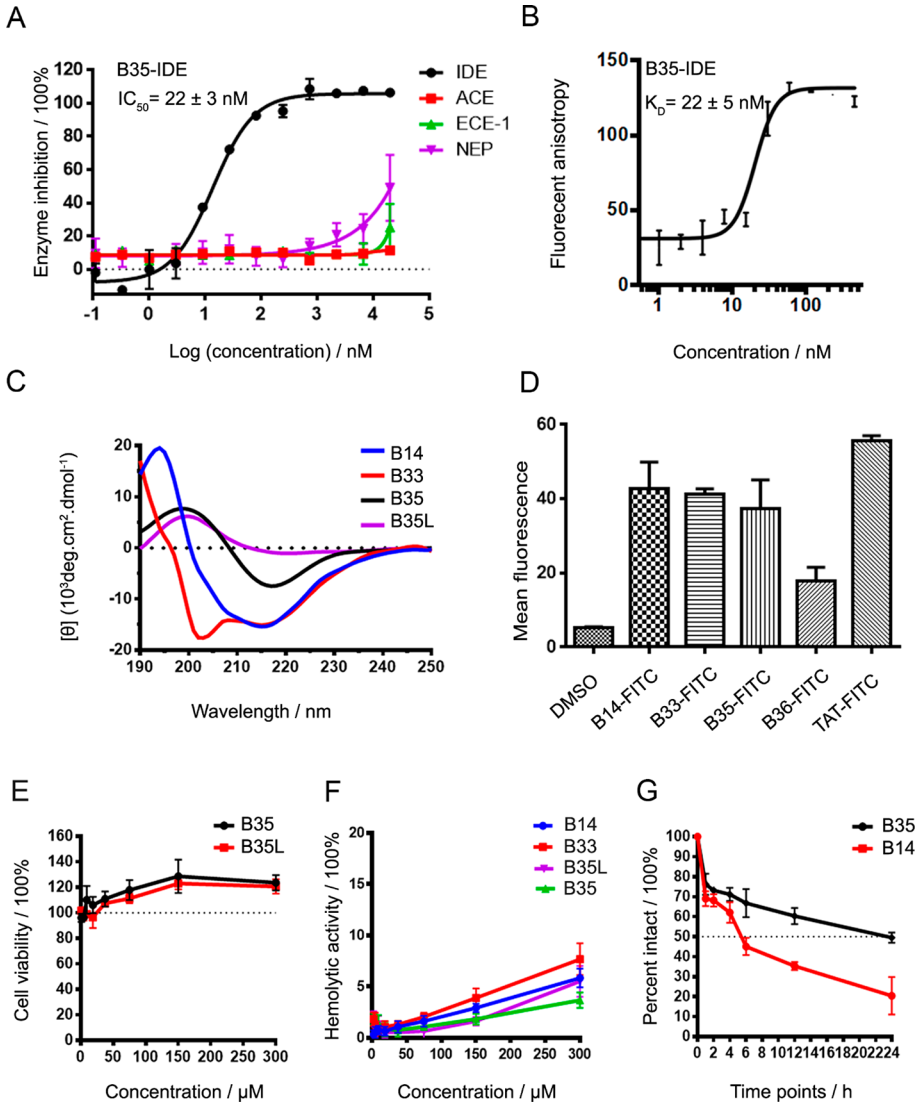

Figure 2. Characterization of peptides *in vitro*. (A) Half maximal inhibitory concentration (IC_{50} = 22 ± 3 nM) of peptide **B35** in protease assays. **B35** peptide showed ≥1000-fold selectivity for inhibition of IDE over other metalloproteases tested (ACE, ECE-1, and NEP, purchased from R&D). Protease inhibition activity was assayed by following cleavage of the fluorogenic peptide substrate Mca-RPPGFSAFK(Dnp)−OH (R&D). (B) Binding affinity of **B35** with IDE-E111Q (K_D = 22 ± 5 nM) using fluorescence polarization assays at 293 K. (C) CD spectra of peptides **B14**, **B33**, and **B35** and scrambled peptide **B35L** in water at 298 K. The data of CD spectra were smoothed using Pro-Data Viewer by Applied Photophysics. (D) Flow cytometry assays using HeLa cells treated with **B14**-FITC, **B33**-FITC, **B35**-FITC, **B36**-FITC, and cell-penetrating peptide **TAT**-FITC (5 μM, 2h, 310 K). (E) MTT assay of **B35** in HeLa cells. HeLa cells were incubated with serial dilution of peptides (from 300 μM) in 5% FBS containing media supplied with 5% CO_2 at 310 K for 24 h. (F) Hemolytic activity curves of peptides. The hemoglobin release was detected by microplate reader at 576 nm. (G) Serum stability of peptide **B35**. Peptides were added to 25% mouse serum to a final concentration of 250 μM, then mixtures were incubated at different time points and the supernatant were measured by LC−MS. Data were shown as mean ± SEMs. SEMs were shown as error bars in the figures.

secondary structures, while **B33** was found to possibly adopt some helical features. The scrambled and linear peptide **B35L** (H-EFLWAG^{D}P^{L}PYACVGRLE-NH_2) was found to exist as a random coil based upon its CD spectrum (Figure 2C). Flow cytometry measurements (Figure 2D) and confocal imaging (Supporting Information, Figure S2) showed that the peptide **B35** had good permeability in HeLa cells. HeLa cells were treated with peptide **B35**-FITC for 2 h, washed with PBS and 0.4% trypan blue, then digested with trypsin, washed, lysed, and examined with LC−MS. Intact peptide **B35**-FITC was detected (Supporting Information, Figure S3).

Peptide toxicity and serum stability were then analyzed in order to further study their therapeutic potential. **B35L** (linear analogue of **B35**) was used as control peptide. Peptide **B35** and **B35L** did not exhibit any obvious toxicity at concentrations below 300 μM (Figure 2E). Besides, peptides **B14**, **B33**, **B35**, and **B35L** showed low hemolytic activity (below 10%) at concentration of 300 μM (Figure 2F; Supporting Information, Figure S4). In the serum stability assay, approximately 50% of peptide **B35** remained intact in 25% mice serum after 24 h, while peptide **B14** was found to be degraded more rapidly (Figure 2G). These results emphasized the necessity of the amide bridged macrocyclization.

In order to evaluate the secondary structure of peptide **B35**, 1D and 2D NMR measurements of peptide **B35** were performed (Supporting Information, Figure S5−S7). The NOE (nuclear Overhauser effect) signals would enhanced when the distance between two protons is less than 5 Å.[55] The

DOI: 10.1021/acs.jmedchem.8b00418
J. Med. Chem. 2018, 61, 8174−8185

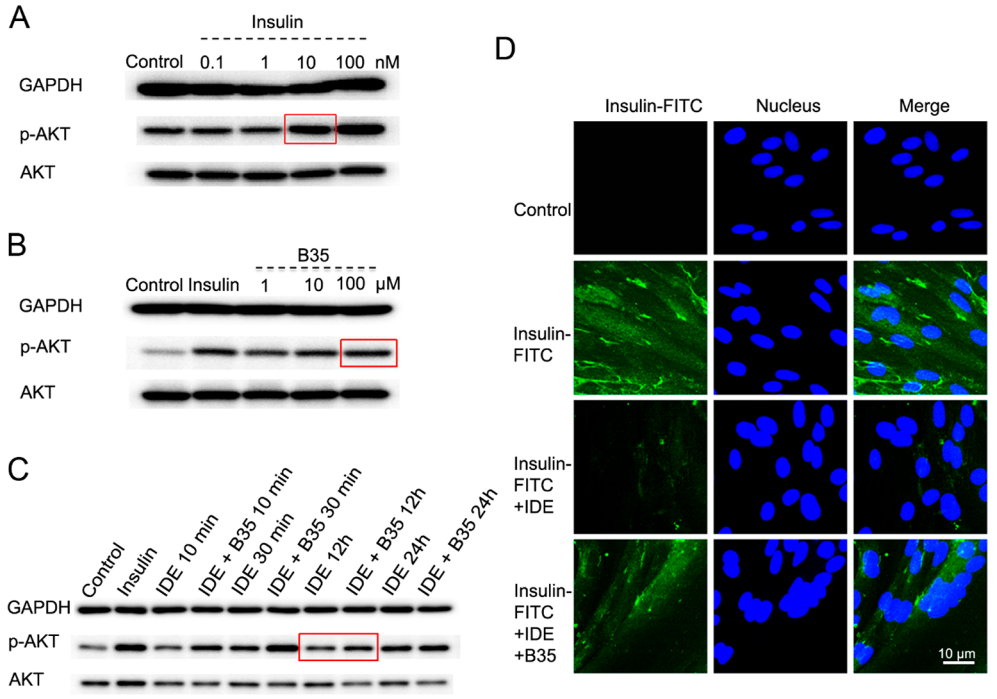

Figure 3. Characterization of peptide **B35** in insulin-induced phosphorylated AKT (pAKT) signaling pathway and the cellular-based degradation study. (A) Western blot analysis of pAKT induced by different concentrations of insulin. (B) Effects of different concentrations of peptide **B35** on the block of IDE inhibition to insulin signaling in skeletal muscle cells. (C) Inhibition efficiency of peptide **B35**. Skeletal muscle cells were treated with 100 nM IDE and 100 μM **B35** at various time points (10 min, 30 min, 12 h, and 24 h), then 10 nM insulin was treated for 10 min to induce the pAKT signaling. (D) Fluorescence of skeletal muscle cells preloaded with FITC-insulin, in the presence/absence of IDE and **B35**. Scale bar: 10 μm.

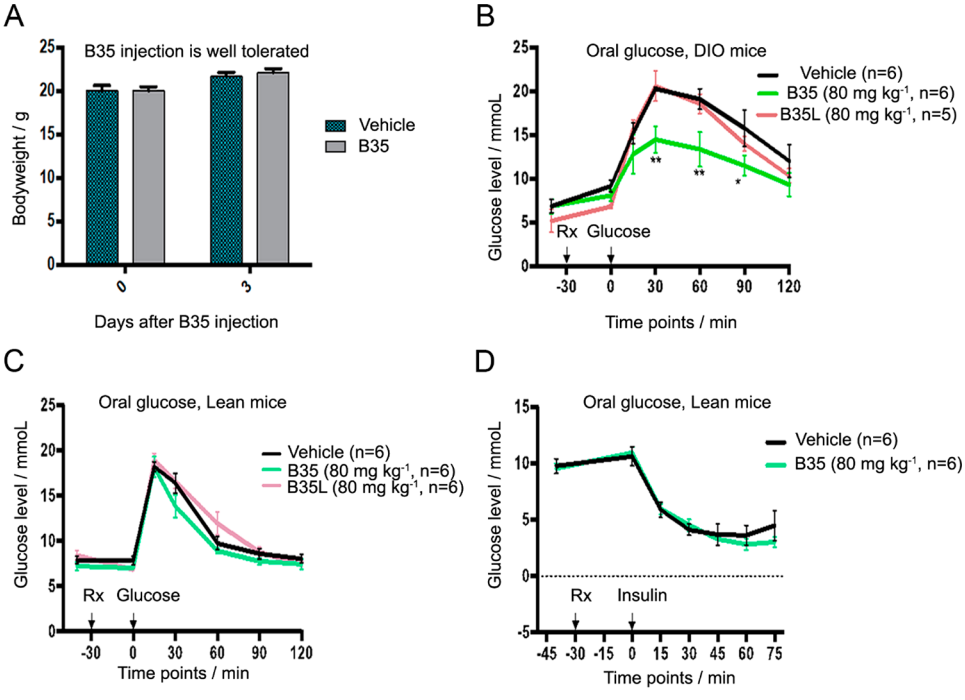

Figure 4. Oral glucose tolerance and insulin tolerance test during acute IDE inhibition. (A) Body weight changes of male C57BL/6J lean mice treated with **B35** (80 mg kg^{-1}, n = 6, i.p. injection) or vehicle (PBS, n = 6, i.p. injection). (B,C) Male DIO mice and male lean C57BL/6J mice were treated with a single i.p. injection of peptide **B35** (80 mg kg^{-1}, n = 6), peptide **B35L** (80 mg kg^{-1}, n = 5 or 6), or vehicle (PBS, n = 6), 30 min before glucose gavage (2.0 g kg^{-1}). (D) Blood glucose responses to insulin in male lean C57BL/6J mice 30 min following treatment with peptide **B35** (80 mg kg^{-1}, n = 6, i.p. injection) or vehicle (PBS, n = 6, i.p. injection). Blood glucose was measured at time points −30, 0, 15, 30, 45, 60, 75, 90, 105, and 120 min corresponding to the time of glucose injection or insulin injection (defined as 0 min) using blood glucose meters and blood glucose test strips. Data were shown as mean ± SEM. SEMs were shown as error bars in the figures. *P < 0.05, **P < 0.01 in two-tail Student's t test.

DOI: 10.1021/acs.jmedchem.8b00418
J. Med. Chem. 2018, 61, 8174−8185

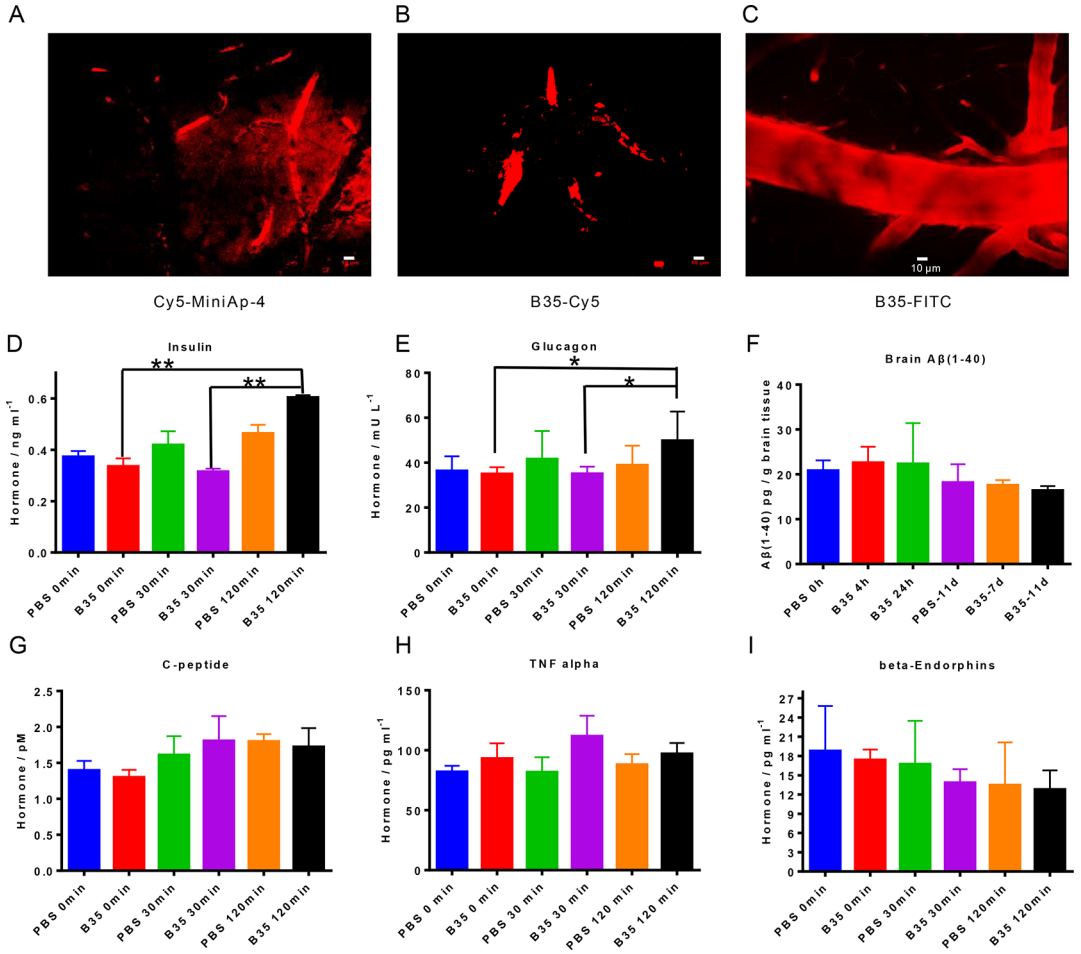

Figure 5. Physiological consequence of **B35** *in vivo*. (A–C) Images of brain vessel or tissue of C57BL/6J mice injected (i.v.) with Cy5 miniAp-4 (A, 40 mg kg^{-1}, red), **B35**-Cy5 (B, 40 mg kg^{-1}, red), or **B35**-FITC (C, 80 mg kg^{-1}; the color was modified from green to red for comparison) were obtained using an Olympus two-photon microscope (FV1000MPE). Cy5 miniAp-4 could across the blood–brain barrier, and it was detectable in brain tissue outside of the brain vessel (A), but **B35**-Cy5 (B) or **B35**-FITC (C) was undetectable in brain tissue. Scale bars: 10 μm. (D,E) Treatment of C57BL/6J lean mice with **B35** (80 mg kg^{-1}, n = 5, i.p. injection) could improve the levels of insulin (**P < 0.01) and glucagon (*P < 0.05) compared to vehicle controls (PBS, n = 5, i.p. injection) 30 or 120 min postinjection. (F) Treatment of C57BL/6J male lean mice with **B35** did not influence brain levels of Aβ (1–40) peptides in brain tissue 4 h, 24 h, 7 days, or 11 days (**B35**, 80 mg kg^{-1}, n = 5, i.p. injection per another day) postinjection compared to treatment with vehicle alone (PBS, n = 5, i.p. injection per another day). (G–I) Treatment of C57BL/6J lean mice with **B35** (80 mg kg^{-1}, n = 5, i.p. injection) did not significantly change basal hormone levels (C-peptide, TNF alpha, beta-endorphins) compared to vehicle controls (PBS, n = 5, i.p. injection) 30 or 120 min postinjection. Data were shown as mean ± SEM. SEMs were shown as error bars in the figures. Statistics were carried out using a two-tail Student's t test with GraphPad Prism 6.0. The significance levels were shown as *P < 0.05 and **P < 0.01.

conformation of peptide **B35** in solution could be confirmed by specific signals such as the cross-peaks of αN(i, i + 1), αN(i, i + 2), and NN(i, i + 1), including the αN(i, i + 1) cross-peaks in residues Glu1-Phe4 and Glu9-Tyr12, the αN(i, i + 2) cross-peaks between the residue Arg3-Asp5 (Supporting Information, Figure S6), as well as the NN(i, i + 1) cross-peaks in residues Glu1-Phe4, Glu9-Dap10, and Val14-Cys15, respectively (Supporting Information, Figure S7). Because of the signal overlap, the cross-strand NOE peaks between Gly6 and Glu9, or Phe4 and Leu11 cannot be confirmed clearly according to the NMR data, which may be considered as important evidence for beta-hairpin structure.[56] The conformation of peptide **B35** may be considered as hypothesized beta-hairpin structures. The chemical shift assignments of **B35** backbone atoms were summarized in Table S3 (Supporting Information).

Skeletal muscle cells were used to test the effects of peptide **B35** on insulin signaling of the AKT phosphorylation pathway. In order to explore the appropriate insulin concentrations required to induce the AKT phosphorylation pathway, we tested 0.1, 1, 10, and 100 nM insulin. The results demonstrated that stimulation with insulin (10 nM) could induce a significant increase in AKT phosphorylation, which is consistent with the previous finding (Figure 3A; Supporting Information, Figure S8A).[57] Western blot results suggested that insulin signaling could be significantly potentiated through the inhibition of IDE proteolytic activity using 10 μM peptide **B35**. IDE was found to completely lose its degradation activity in the presence of 100 μM peptide **B35** compared to insulin positive control (Figure 3B; Supporting Information, Figure S8B). In addition, a time gradient assay demonstrated that inhibition effects could last for up to 12 h in the presence of 100 μM peptide **B35** (Figure 3C; Supporting Information, Figure S8C).

Wild type IDE can rapidly degrade insulin *in vitro* (Supporting Information, Figures S9 and S10). We next

DOI: 10.1021/acs.jmedchem.8b00418
J. Med. Chem. 2018, 61, 8174–8185

A

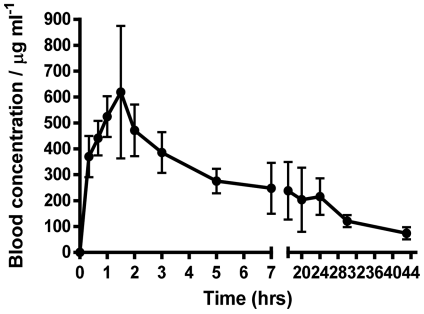

B

Parameters	Mean±SEM
T_{max} (hours)	1.4±0.5
C_{max} (μg/mL)	618.9±157.3
$AUC_{0\text{-}43h}$ (mg*hours/mL)	7.6±1.1
F_{abc} (%)	83.5±9.8

Figure 6. *In vivo* pharmacokinetic properties of **B35** peptide. (A) Average mean blood concentration−time plot of **B35** in C57BL/6J lean mice after intraperitoneal injection (100 mg kg^{-1}, n = 5). (B) *In vivo* pharmacokinetic parameters of **B35** via intraperitoneal intravenous injection (100 mg kg^{-1}, n = 5). In different time points postinjection, peptides remaining in the supernatant of plasma were determined by LC−MS. Data were shown as mean ± SEM. SEMs were shown as error bars in the figure.

studied the influence of peptide **B35** on the cellular-based degradation of FITC-labeled insulin. Skeletal muscle cells were treated with different concentrations of FITC-insulin, IDE, and **B35**, and the fluorescent intensity was monitored. Upon treatment of cells with 100 nM FITC-insulin, fluorescence was clearly observed within 10 min (Figure 3D). In the presence of 100 nM IDE, cells showed low fluorescence, as FITC-insulin was rapidly degraded. Intracellular fluorescence was found to remain when 100 nM IDE and 100 μM peptide **B35** were added simultaneously. This experiment verified the inhibition of peptide **B35** on the IDE degradation efficiency.

Next, both lean and diet-induced obese (DIO) mouse models (Supporting Information, Figure S11) were used to further evaluate the ability of **B35** to inhibit IDE activity *in vivo*. The peptide **B35** (80 mg kg^{-1}, n = 6, i.p. injection) was found to be well tolerated in lean mice, with no obvious behavioral or postexperiment body weight changes observed (Figure 4A). DIO mice function as a suitable model for early type-2 diabetes in humans as they exhibit hyperinsulinemia and insulin resistance. During oral glucose tolerance tests (OGTTs), **B35**-treated (80 mg kg^{-1}, n = 6, i.p. injection) DIO mice were found to demonstrate significantly improved glucose tolerance relative to both vehicle (PBS, n = 6, i.p. injection) and **B35L** (80 mg kg^{-1}, n = 5, i.p. injection) treated mice (Figure 4B). Vehicle and **B35L** control groups were found to exhibit similar blood glucose profiles. However, lean mice treated with **B35** (80 mg kg^{-1}, n = 6, i.p. injection) did not exhibit a statistical difference in glucose tolerance relative to control groups (Figure 4C). We next injected insulin 30 min after **B35** or vehicle treatment. We observed that **B35**-treated (80 mg kg^{-1}, n = 6, i.p. injection) male lean mice demonstrated hypoglycemia during insulin tolerance tests (ITTs, Figure 4D).

It is worth mentioning that **B35** was undetectable in brain parenchyma compared to permeable peptidomimetic Cy5 miniAp-4,[58] which suggested **B35** will not interrupt IDE's function in brain (Figure 5A−C). Treatment of C57BL/6J lean mice with **B35** (80 mg kg^{-1}, n = 5, i.p. injection) could improve the levels of insulin and glucagon (Figure 5D,E) but did not significantly change Aβ peptide or other basal hormone levels (C-peptide, TNF alpha, beta-endorphins) compared to vehicle controls (PBS, n = 5, i.p. injection) (Figure 5F−I). In addition, the average mean blood concentration−time plot of **B35** and pharmacokinetic properties of **B35** *in vivo* (T_{max}, 1.4 ± 0.5 h; C_{max}, 618.9 ± 157.3 μg/mL; AUC_{0-43h}, 7.6 ± 1.1 mg·h/mL; F_{abc}, 83.5% ± 9.8%) are summarized in Figure 6.

Using the originally developed amide bond cyclization methodology, we mimicked the β-sheet conformation of insulin B chain and developed effective peptide inhibitors of IDE. The peptide IDE inhibitor **B35** could be prepared facially using standard solid phase peptide synthesis and shows a half-maximum inhibitory concentration of 22 nM with very little toxicity and good serum stability. Insulin signaling can be significantly potentiated through the inhibition of IDE proteolytic activity using the inhibitor **B35**. DIO mice treated with **B35** (80 mg kg^{-1}, n = 6, i.p. injection) demonstrated improved glucose tolerance, consistent with findings from Saghatelian and Liu et al. with **6bk**. In order to further assess the capability of **B35** to mediate insulin degradation *in vivo*, we carried out ITT experiments in lean mice. Insulin sensitization was found to be elevated but did not reach statistical significance. In summary, the inhibitor **B35** represents a novel candidate that can be used for the further study of IDE functions.

CONCLUSIONS

The development of the physiologically active IDE inhibitor **B35** was based on a dual β-hairpin stabilizing strategy. This included a ^{D}Pro-^{L}Pro nucleating turn combined with a precisely positioned amide bond. In *in vitro* studies, the peptide exhibited a good inhibition efficacy, low toxicity, and an ideal serum stability. We have confirmed its competition with insulin at the cellular level and have proven its influence on the insulin signaling pathway. We demonstrate that peptide **B35** is able to improve glucose tolerance in an obese mouse model under conditions that mimic meal intake. This study provides a good basis for the further development of potent IDE peptide inhibitors.

EXPERIMENTAL SECTION

Materials. All solvents and reagents were used directly without further purification unless otherwise stated. The solvents and reagents were purchased from commercial suppliers including GL Biochem (Shanghai) Ltd., Shanghai Hanhong Chemical Co., J&K Co. Ltd., Shenzhen Tenglong Logistics Co., or Energy Chemical Co. All chemicals used for protein expression and purifications were purchased from Sigma-Aldrich and Fisher.

Synthesis of IDE Peptides. Peptides were synthesized on Rink amide MBHA resin using manual Fmoc/*t*Bu solid-phase peptide synthesis (SPPS). First, the Fmoc group on the resin was removed by treatment with 50% (v/v) morpholine/NMP for 1 h. Then wash the resin with DCM, DMF, and NMP alternately for 6 times, and add

DOI: 10.1021/acs.jmedchem.8b00418
J. Med. Chem. 2018, 61, 8174−8185

Fmoc-protected amino acids (5 equiv), HCTU (5 equiv), DIPEA (10 equiv) reagents in DMF for coupling reactions with N_2 bubbling for 2 h. The allyl ester and allyl carbamate were removed using $Pd(PPh_3)_4$ (0.1 equiv) and 1,3-dimethylbarbituric acid (4 equiv) in anhydrous DCM for 2 h for 2 times. Cyclization was performed on the resin using PyBOP/HOBt/NMM (2:2:2.4 equiv) in DMF with N_2 bubbling for 4 h. The synthesis routes for peptides are shown in Schemes S1 and S2 in the Supporting Information. FITC labeling was performed with the solution of FITC (isomer I, 4 equiv) and DIPEA (14 equiv) in DMF on the resin overnight. Cy5 labeling was performed with the solution of Cy5 NHS Ester (2 equiv, Beijing Okeanos Technology Co., Ltd.) and DIPEA (4 equiv) in DMF on the resin for 24 h. At last, resins were treated with methanol for 10 min and then dried with N_2. Resins were treated with the solution of TFA/TIS/H_2O ($V_{TFA}/V_{TIS}/V_{H2O}$ (%) = 95:2.5:2.5) for 2 h. After removing most of the TFA with N_2, crude products were precipitated with diethyl ether, then dissolved in 50% (v/v) CH_3CN/H_2O. Crude peptides were then purified on RP-HPLC (SHIMAZU Prominence LC-20AT).

HPLC and Mass Spectrometry.[59] Crude peptides were purified by RP-HPLC (SHIMAZU Prominence LC-20AT) with a C18 analytic column (Agilent Zorbax SB-Aq, 4.6 × 250 mm, 5 μm, flow rate 1.0 mL/min). Pure water (containing 0.1% TFA) and pure acetonitrile were used as mobile phase. LC−MS analysis was performed on LC−MS 8030 (SHIMAZU LC−MS 2020 mass-spectrometer, Agilent Zorbax SB-Aq: 4.6 × 250 mm, 495 nm). The purity of the peptides were confirmed by analytic HPLC and mass spectrometry, and all the final peptides were ≥95% purity (Supporting Information, Figure S12, Table S2).

Protease Assays with Fluorogenic Peptide Substrates.[21] Using the fluorophore/quencher-tagged peptide substrate Mca-RPPGFSAFK(Dnp)−OH (R&D) to detect $IDE_{42-1019}$ proteases, the buffer contained 50 mM Tris pH 7.5, 1 M NaCl. Angiotensin-converting enzyme (ACE, R&D), endothelin-converting enzyme-1 (ECE-1, R&D), and neprilysin (NEP, R&D) were assayed according to the manufacturer's protocol and recommended buffers using the same peptide substrate Mca-RPPGFSAFK(Dnp)−OH (R&D). First, 48 μL of $IDE_{42-1019}$ enzyme mixtures (0.2 μg/mL) were transferred to a 96-well black plate. Two microliters of **B35** peptide was then added in a 3-fold dilution manner (concentration of the peptides began from 20 μM). Mixtures were allowed to equilibrate for 10 min. Subsequently, 50 μL of peptide substrate (20 μM) was added to initiate the enzymatic reaction. Finally the mixtures were mixed well and monitored on a fluorescence plate reader within 5 min (excitation at 340 nm, emission at 405 nm). The data points were obtained from four independent experiments with each performed in duplicate.

Fluorescence Polarization Assay.[60] Fluorescence polarization (FP) assays were performed in 96-well black plates. Concentrations of the peptides were determined by 494 nm absorption of FITC. Purified IDE-E111Q and 20 nM FITC-labeled peptide were mixed and incubated at 277 K for 2 h in the dark. The buffer contains 20 mM Tris-HCl pH 8.0, 50 mM NaCl, and 1 mM TCEP. The fluorescence polarization of the labeled peptide was measured using a plate reader (PerkinElmer) with excitation at 480 nm and emission at 535 nm at 298 K and then plotted against the concentrations of the IDE. The data were analyzed using GraphPad Prism 6.0. Representative data points were obtained from three independent experiments with each performed in duplicate.

Circular Dichroism Spectroscopy.[61] CD spectra were acquired using circular dichroism spectrometer (Chirascan-Plus) equipped with a temperature controller. Peptide samples were dissolved in pure water with the final concentration between 0.5 to 1 mM, then the CD spectra were acquired using a 1 mm cell at a scan speed of 20 nm/s at 298 K. Each peptide sample was scanned twice, and the averaged spectrum was smoothed. Final concentrations of the peptides were measured by 280 nm absorption of Tyr or Trp on the peptides. The experiments were repeated for three times.

Flow Cytometry Analysis.[50] HeLa cells were seeded in 24-well plates and allowed to grow overnight in high-glucose Dulbecco's modified Eagle's medium (DMEM, Gibco), supplemented with 10% (v/v) fetal bovine serum (FBS, Gibco BRL) and 1% penicillin/streptomycin (pen/strep, Gibco) at 310 K with 5% CO_2 in a humidified incubator. HeLa cells were treated with 5 μM FITC-labeled peptides in FBS-free medium for 2 h at 310 K. The peptide solution was removed, and cells were washed with phosphate-buffered saline (PBS) and 0.4% trypan blue, the cells were harvested by digesting with trypsin (Gibco), then washed with PBS for three times. Cellular mean fluorescence intensities were measured using a FACS calibur flow cytometer (Becton Dickinson, Mississauga, CA). The transfection efficiency of peptides was assessed by calculating the number of cells in a specified gate. Representative data points were obtained from three independent experiments.

Cell Viability Assay. HeLa cells were seeded in 96-well plates and allowed to grow in DMEM medium supplemented with 10% FBS overnight. The cells were incubated with serial dilution of peptides (from 300 μM) in 5% FBS containing media supplied with 5% CO_2 at 310 K for 24 h. Subsequently, 20 μL of MTT reagent was added to each well. Cells were incubated at 310 K for another 4 h. The absorbance of formazan product was measured at 490 nm with a microplate reader (PerkinElmer). Representative data points were obtained from three independent experiments with each performed in duplicate.

Hemolytic Activity Test.[62] Hemolytic activity tests were performed with fresh red blood cells of mouse. The fresh red blood cells were washed with PBS for 6 times, and then diluted in the concentration of 1×10^8 cells/mL in PBS. The peptides **B14**, **B33**, **B35**, and **B35L** were added into the red blood cell suspension at gradient concentrations of 300.0, 150.0, 75.0, 37.5, 18.8, 9.4, 4.7, and 2.3 μM in 1.5 mL tubes. Next, the mixtures were incubated at 310 K for 1 h. After incubation, the mixtures were centrifuged for 1 min at a speed of 8600 rpm, the supernatant was transferred into a 96-well plate, and the hemoglobin release was measured at 576 nm using a microplate reader (TECAN, Switzerland). In this assay, 0.1% Triton-X 100 and PBS were used as the positive control and negative control, respectively. The data points were obtained from three independent experiments with each performed in duplicate. The efficiency of hemolysis was calculated by the following equation:

$$\begin{aligned}\text{hemolysis}(\%) = [&(OD_{576}\text{nm of exptl sample} \\ &- OD_{576}\text{nm of negative control})/(OD_{576}\text{nm of the positive control} \\ &- OD_{576}\text{nm of negative control})] \times 100\%\end{aligned}$$

***In Vitro* Serum Stability.**[28] Peptides were added to 25% mouse serum to a final concentration of 250 μM at final volume of 100 μL. Samples were incubated at 310 K for 0, 1, 2, 4, 6, 12, and 24 h, respectively. After incubation, 50 μL of each sample was added to 120 μL of buffer S (12% TCA in H_2O/CH_3CN (1:1) solution), followed by cooling to 277 K for 15 min to precipitate serum proteins. After centrifugation (13,000 rpm, 277 K, 10 min), peptides remaining in the supernatant were determined by LC−MS. Representative data points were obtained from three independent experiments.

Western Blot Analysis.[63−65] Rat skeletal muscle cells were the kind gifts of Prof. Peter CY Tong in Chinese University of Hong Kong[66,67] and were incubated in the lab of Prof. Lizhong Liu in School of Medicine, Shenzhen University, Guangdong, China. For insulin-induced phosphorylated AKT (pAKT) signaling study, skeletal muscle cells were seeded in 6-well plates and treated with 100 nM IDE and incubated with **B35** peptide for 10 min. In addition, to assess the inhibitory effects on the peptide **B35**, cells were treated with 100 nM IDE and 100 μM **B35** at various time points with 10 nM insulin added for 10 min to induce the pAKT signaling. Then 10 nM insulin was treated for 10 min to induce the pAKT signaling. To isolate protein, cells were washed with PBS for 3 times and harvested using the lysis buffer (RIPA, BioTeke) supplemented with 0.01% protease inhibitor mixture and 0.5 mM phosphatase inhibitor, followed by centrifugation at 6000 rpm for 15 min at 277 K. Total cellular protein concentrations were determined using Bicinchoninic Acid (BCA) Kit (Sigma-Aldrich). Cell extracts were resolved using 10% SDS-PAGE gel. Protein bands in the gel were then transferred onto a polyvinylidene difluoride (PVDF) membrane by electrophoresis.

DOI: 10.1021/acs.jmedchem.8b00418
J. Med. Chem. 2018, 61, 8174−8185

The antibodies dilution ratio were as follows: 1:1000 for pAKT (Cell Signaling, Beverly, MA, USA) and 1:1000 for AKT (Cell Signaling). GAPDH (diluted at 1:2000, Cell Signaling) was used as a loading control. Membranes were incubated overnight at 277 K and washed for 3 times. HRP-conjugated goat antirabbit IgG antibodies were used for secondary incubation for 1 h at room temperature. Proteins on the membranes were then visualized using chemiluminescent substrates. Data were shown as mean ± SEM in Figure S8 in the Supporting Information. SEMs were shown as error bars in the figures. Statistics were carried out using a two-tail Student's *t* test with GraphPad Prism 6.0. The significance levels were shown as $^*P < 0.05$ and $^{**}P < 0.01$. The data were considered statistically significant when $^*P < 0.05$. Three independent regions from corresponding Western spots were obtained, and area densities were analyzed by Gel-Pro analyzer 4.

Fluorescent Inverted Microscope Imaging.[68] Skeletal muscle cells were seeded on the coverslips in 24-well plates overnight, then added 100 nM wild type IDE protein and 100 μM **B35** peptide. After 10 min incubation at 310 K, the skeletal muscle cells were treated with insulin (labeled with FITC) for another 10 min. Media were removed followed by washing with phosphate buffered saline (PBS) for three times. Cells were then fixed by adding 4% paraformaldehyde for 15 min at 310 K. Nuclei were stained with 4′,6-diamidino-2-phenylindole (DAPI) for 5 min, and cells were mounted on slides to be visualized with fluorescent inverted microscope (Olympus). The experiments were repeated for three times.

***In Vivo* Studies, General Information.** Wild type C57BL/6J male lean adult mice were purchased from the Medical Laboratory Animal Center of Guangdong Province, People's Republic of China. Diet-induced obese (DIO) C57BL/6J male adult mice were the kind gifts of Prof. Peigen Ren in Shenzhen Institutes of Advanced Technology (SIAT, China) (Supporting Information, Figure S11). The lean mice were 13 to 15 weeks old, and DIO mice were 22 to 26 weeks old (Supporting Information, Figure S11C). All lean mice were housed individually on a 14 h light, 10 h dark schedule at the School of Chemical Biology and Biotechnology, Peking University. DIO mice were housed individually in Shenzhen Institutes of Advanced Technology (SIAT, China). Water and food were available, including normal chow diet for lean mice and high-fat diet (45 kcal% fat, D12451, Research Diets Inc.) for DIO mice. The animals were divided into groups randomly for subsequent experiments.

All experiments in lean mice were carried out in accordance with the National Standard of Animal Care and Use Procedures at the Laboratory Animal Center of Peking University Shenzhen Graduate School, Guangdong Province, People's Republic of China (the permit number is IACUC-ER-0023-005). All experiments in DIO mice were carried out in accordance with the National Standard of Animal Care and Use Procedures at the Laboratory Animal Center of Shenzhen Institutes of Advanced Technology, Guangdong Province, People's Republic of China (the permit number is SY59434, the ethic number is SIAT-IRB-150128-YGS-YZY-A0087-1).

Glucose Tolerance Tests (GTT) and Blood Glucose Measurements.[21] Before glucose stimulation, the animals were fasted for 16 h (8 PM to 12 AM, during the dark cycle), while individuals were housed in a clean cage with inedible plastic-chip as a plastic substrate, bits of wood, and a white plastic hut. **B35** peptide inhibitor (80 mg kg^{-1}, $n = 6$), vehicle (PBS, $n = 6$), or negative control **B35L** random sequence peptide (80 mg kg^{-1}, $n = 5$ for DIO mice and $n = 6$ for lean mice) were administered by a single intraperitoneal (i.p.) injection 30 min prior to the glucose stimulation. Twenty percent dextrose was dissolved in PBS, and the dose was adjusted by fasted body weight of animals. Dextrose (2.0 g kg^{-1}) was administered by gavage. Blood glucose was measured using blood glucose meters and blood glucose test strips (Roche Diagnostics GmbH) from blood droplets, which were acquired from a small incision of the tail. Blood glucose was measured at time points −30, 0, 15, 30, 45, 60, 75, 90, 105, and 120 min corresponding to the time of glucose injection (defined as 0 min). Blood glucose values were shown as mean ± SEM. SEMs were shown as error bars in the figures. Statistics were carried out using a two-tail Student's *t* test with GraphPad Prism 6.0. The significance levels were shown as $^*P < 0.05$ and $^{**}P < 0.01$ versus vehicle control group. The data were considered statistically significant when $^*P < 0.05$. The experiments were repeated for four times.

Insulin Tolerance Tests (ITT).[21] For insulin challenges, lean mice were fasted individually housed as described above. Animals were fasted for a period of 6 h (7 AM to 1 PM). Lean mice were distributed randomly into two groups (six mice per group) and were subcutaneously injected i.p. with vehicle (PBS, $n = 6$) or **B35** peptide (80 mg kg^{-1}, $n = 6$), 30 min prior to each insulin challenge. Insulin (Sigma), which was formulated in sterile saline (5 mL kg^{-1}), was injected subcutaneously (0.25 U kg^{-1}). Blood glucose was measured at time points −30, 0, 15, 30, 45, 60, and 75 min, which reference the time of insulin injection (defined as 0 min), by microsampling from a tail nick of the animals. Blood glucose values were shown as mean ± SEM. SEMs were shown as error bars in the figures. Statistics were carried out using a two-tail Student's *t* test with GraphPad Prism 6.0. The significance levels were shown as $^*P < 0.05$ and $^{**}P < 0.01$ versus vehicle control group. The data were considered statistically significant when $^*P < 0.05$. The experiments were repeated for three times.

Microscopy Imaging of Brain Tissue.[58,69] To image brain vessel and tissue in awake state using head-restrained C57BL/6J mice, the head-holder of mice was fixed to two metal solids. Using the high-speed microdrill and microsurgical blade to thin the skull to a thickness of approximately 20 μm. Then Cyanine5 conjugates (Cy5 miniAp-4, **B35**-Cy5, 40 mg kg^{-1}) and **B35**-FITC (80 mg kg^{-1}) were injected via orbital intravenous injection (i.v.) in C57BL/6J lean mice. The head-restrained mice were then placed on the microscope stage. Image stacks were obtained using an Olympus two-photon microscope (FV1000MPE) with the laser tuned to 920 nm and with a 1.05 N.A. A 25× objective was immersed in artificial cerebrospinal fluid. A 3× digital zoom was used to acquire high-magnification images (169 μm × 169 μm, 1024 × 1024 pixels for 25 × objective) of brain vessel and tissue.

Amyloid Peptide Measurements.[21] C57BL/6J lean mice were treated with **B35** peptide (80 mg kg^{-1}, $n = 5$, i.p. injection per another day) and vehicle (PBS) alone. Brain tissues (~350 mg wet weight) were homogenized in a Dounce homogenizer in PBS containing 1 mM PMSF. Then the homogenate was centrifuged at 13,000 rpm for 30 min at 277 K, and the supernatant (50 μL) was analyzed for Aβ (1−40) levels using the Aβ (1−40) ELISA assays (Jianglaibio, China) according to the manufacturer's introduction. Data were shown as mean ± SEM. SEMs were shown as error bars in the figures. Statistics were carried out using a two-tail Student's *t* test with GraphPad Prism 6.0. The significance levels were shown as $^*P < 0.05$ and $^{**}P < 0.01$. The data were considered statistically significant when $^*P < 0.05$. Representative data points were obtained from two or more independent experiments with each performed in duplicate.

Blood Collection and Plasma Hormone Measurements.[21] **B35** peptide (80 mg kg^{-1}, $n = 5$) were injected via intraperitoneal (i.p.) injection in C57BL/6J male lean mice. After 30 or 120 min, blood was collected in EP tubes containing 10 μL of 0.1% heparin sodium. The blood was acquired from a small incision of the tail or the mice eye socket. Then the blood was centrifugated 20 min at 5000 rpm to separate the plasma and red blood cells. The plasma was aliquoted, flash frozen over liquid nitrogen, and stored at −80 °C. According to the manufacturer's protocols, insulin was quantified from 5 μL of plasma supernatant using Ultra Sensitive Mouse Insulin ELISA Kit (Crystal Chem). C-Peptide fragment was quantified from 10 μL of plasma supernatant using Ultrasensitive ELISA Kit (ALPCO). Glucagon and beta-endorphins were quantified from 10 μL of plasma supernatant using Ultrasensitive ELISA Kit (Dogesco). TNF alpha was quantified from 10 μL of plasma supernatant using Ultrasensitive ELISA Kit (Alpha Diagnoestic International). Data were shown as mean ± SEM. SEMs were shown as error bars in the figures. Statistics were carried out using a two-tail Student's *t* test with GraphPad Prism 6.0. The significance levels were shown as $^*P < 0.05$ and $^{**}P < 0.01$. The data were considered statistically significant when $^*P < 0.05$. Representative data points were obtained from two or more independent experiments with each performed in duplicate.

DOI: 10.1021/acs.jmedchem.8b00418
J. Med. Chem. 2018, 61, 8174−8185

Absolute Bioavailability and Determination of Pharmacokinetic Properties of B35.[70] *In vivo* pharmacokinetic properties of **B35** via intraperitoneal injection (i.p., 100 mg kg^{-1}, $n = 5$) determined in different time points postinjection. The absolute bioavailability (F_{abc} %) of **B35** (80 mg kg^{-1}, $n = 5$) via orbital intravenous injection (i.v., assumed as 100%) and intraperitoneal injection (i.p.) in different time points postinjection. The blood was acquired from a small incision of the tail or the mice eye socket in different time points (20 min, 40 min, 1 h, 1.5 h, 2 h, 3 h, 5 h, 7 h, 17 h, 20 h, 24 h, 30 h, and 43 h), then the blood was centrifuged 20 min at 5000 rpm to separate the plasma and red blood cells. Thirty microliters of each plasma sample was added to 100 μL of buffer S (10% TCA in H_2O/CH_3CN (v/v = 1:1) solution), followed by a cooling to 277 K for 15 min to precipitate serum proteins. After centrifugation (13,000 rpm, 277 K, 10 min), peptides remaining in the supernatant were determined by LC−MS. LC−MS analysis was performed on LC−MS 8030 (SHIMAZU LC−MS 2020 mass-spectrometer, Agilent Zorbax SB-Aq: 4.6 × 250 mm, 495 nm). The data points were obtained from two independent experiments.

The absolute bioavailability (F_{abc} %) was calculated by the following equation:

$$F_{abc}\% = (AUC_{ip} \times D_{iv})/(AUC_{iv} \times D_{ip}) \times 100\%$$

■ ASSOCIATED CONTENT

Supporting Information

The Supporting Information is available free of charge on the ACS Publications website at DOI: 10.1021/acs.jmedchem.8b00418.

Experimental section and characterization of peptides, protease assay, hemolytic activity studies, Western blotting data, HPLC plots, mass data, 2D NMR spectra, blood−brain barrier permeability assay, some pharmacokinetic properties, etc. (PDF)

■ AUTHOR INFORMATION

Corresponding Author

*E-mail: lizg@pkusz.edu.cn.

ORCID

Zigang Li: 0000-0002-3630-8520

Author Contributions

#Y.D. and Q.W. contributed equally to this work.

Notes

The authors declare no competing financial interest.

■ ACKNOWLEDGMENTS

This work supported by High-performance Computing Platform of Peking University. We acknowledge financial support from the Natural Science Foundation of China, grants 21778009 and 81701818, the Shenzhen Science and Technology Innovation Committee, JCYJ20170412150719814 and JCYJ20170413165503382, and the Guangdong Public Research and Capacity Building Special Program, 2015A020212030.

■ ABBREVIATIONS USED

BCA, bicinchoninic acid; CD, circular dichroism; Dap, 2,3-diaminopropionic acid; DAPI, 4′,6-diamidino-2-phenylindole; DCM, dichloromethane; DIC, *N*,*N*′-diisopropylcarbodiimide; DIO, diet-induced obese; DIPEA, *N*,*N*′-diisopropylethylamine; DMEM, Dulbecco's modified Eagle's medium; DMF, *N*,*N*′-dimethylformamide; FACS, fluorescence-activated cell sorting; FBS, fetal bovine serum; FITC, fluorescein isothiocyanate; Fmoc, 9-fluorenylmethyloxycarbonyl; FP, fluorescence polarization; GTT, glucose tolerance tests; HCTU, 2-(1*H*-6-chlorobenzotriazol-1-yl)-1,1,3,3-tetramethyluronium hexafluorophosphate; HOBt, 1-hydroxybenzotriazole; ITT, insulin tolerance test; MBHA, 4-methylbenzylhydrylamine; MS, mass spectrometry; MTT, 3-(4,5)-dimethylthiahiazo(-z-y1)-3,5-diphenytetrazoliumromide; LC−MS, liquid chromatograph−mass spectrometer; NMP, *N*-methyl pyrrolidone; PBS, phosphate buffer saline; PyBOP, benzotriazol-1-yl-oxytripyrrolidinophosphonium hexafluorophosphate; RP-HPLC, reserved-phase high-performance liquid chromatography; SDS-PAGE, sodium dodecyl sulfate-polyacrylamide gel electrophoresis; SPPS, solid-phase peptide synthesis; TCA, trichloroacetic acid; TCEP, tris(2-carboxyethyl)phosphine; TFA, trifluoroacetic acid; TIS, triisopropylsilane; T_{max} (h), time to maximum plasma concentration; C_{max} (μg/mL), peak plasma concentration; AUC (mg·h/mL), area under the concentration−time curve; F_{abc} (%), absolute bioavailability

■ REFERENCES

(1) Banting, F. G.; Best, C. H.; Collip, J. B.; Campbell, W. R.; Fletcher, A. A. Pancreatic extracts in the treatment of diabetes mellitus. *Can. Med. Assoc. J.* **1922**, *12*, 141−146.

(2) Manolopoulou, M.; Guo, Q.; Malito, E.; Schilling, A. B.; Tang, W. J. Molecular basis of catalytic chamber-assisted unfolding and cleavage of human insulin by human insulin-degrading enzyme. *J. Biol. Chem.* **2009**, *284*, 14177−14188.

(3) Kim, Y. G.; Lone, A. M.; Saghatelian, A. Analysis of the proteolysis of bioactive peptides using a peptidomics approach. *Nat. Protoc.* **2013**, *8*, 1730−1742.

(4) Kim, Y. G.; Lone, A. M.; Nolte, W. M.; Saghatelian, A. Peptidomics approach to elucidate the proteolytic regulation of bioactive peptides. *Proc. Natl. Acad. Sci. U. S. A.* **2012**, *109*, 8523−8527.

(5) Baumeister, H.; Müller, D.; Rehbein, M.; Richter, D. The rat insulin-degrading enzyme: molecular cloning and characterization of tissue-specific transcripts. *FEBS Lett.* **1993**, *317*, 250−254.

(6) Tomizawa, H. H. Mode of action of an insulin-degrading enzyme from beef liver. *J. Biol. Chem.* **1962**, *234*, 428−431.

(7) Malito, E.; Hulse, R. E.; Tang, W. J. Amyloid beta-degrading cryptidases: insulin degrading enzyme, presequence peptidase, and neprilysin. *Cell. Mol. Life Sci.* **2008**, *65*, 2574−2585.

(8) Makarova, K. S.; Grishin, N. V. The Zn-peptidase superfamily: functional convergence after evolutionary divergence 1. *J. Mol. Biol.* **1999**, *292*, 11−17.

(9) Shen, Y.; Joachimiak, A.; Rosner, M. R.; Tang, W. J. Structures of human insulin-degrading enzyme reveal a new substrate recognition mechanism. *Nature* **2006**, *443*, 870−874.

(10) Im, H.; Manolopoulou, M.; Malito, E.; Shen, Y.; Zhao, J.; Neant-Fery, M.; Sun, C. Y.; Meredith, S. C.; Sisodia, S. S.; Leissring, M. A.; Tang, W. J. Structure of substrate-free human insulin-degrading enzyme (IDE) and biophysical analysis of ATP-induced conformational switch of IDE. *J. Biol. Chem.* **2007**, *282*, 25453−25463.

(11) Duckworth, W. C.; Bennett, R. G.; Hamel, F. G. Insulin acts intracellularly on proteasomes through insulin-degrading enzyme. *Biochem. Biophys. Res. Commun.* **1998**, *244*, 390−394.

(12) Leissring, M. A.; Farris, W.; Wu, X.; Christodoulou, D. C.; Haigis, M. C.; Guarente, L.; Selkoe, D. J. Alternative translation initiation generates a novel isoform of insulin-degrading enzyme targeted to mitochondria. *Biochem. J.* **2004**, *383*, 439−446.

(13) Leissring, M. A.; Malito, E.; Hedouin, S.; Reinstatler, L.; Sahara, T.; Abdul-Hay, S. O.; Choudhry, S.; Maharvi, G. M.; Fauq, A. H.; Huzarska, M.; May, P. S.; Choi, S.; Logan, T. P.; Turk, B. E.; Cantley, L. C.; Manolopoulou, M.; Tang, W. J.; Stein, R. L.; Cuny, G. D.; Selkoe, D. J. Designed inhibitors of insulin-degrading enzyme regulate the catabolism and activity of insulin. *PLoS One* **2010**, *5*, e10504.

DOI: 10.1021/acs.jmedchem.8b00418
J. Med. Chem. 2018, 61, 8174−8185

(14) Kochkina, E. G.; Plesneva, S. A.; Vasilev, D. S.; Zhuravin, I. A.; Turner, A. J.; Nalivaeva, N. N. Effects of ageing and experimental diabetes on insulin-degrading enzyme expression in male rat tissues. *Biogerontology* **2015**, *16*, 473−484.
(15) Costes, S.; Butler, P. C. Insulin-degrading enzyme inhibition, a novel therapy for type 2 diabetes? *Cell Metab.* **2014**, *20*, 201−203.
(16) Qiu, W. Q.; Walsh, D. M.; Ye, Z.; Vekrellis, K.; Zhang, J.; Podlisny, M. B.; Rosner, M. R.; Safavi, A.; Hersh, L. B.; Selkoe, D. J. Insulin-degrading enzyme regulates extracellular levels of amyloid beta-protein by degradation. *J. Biol. Chem.* **1998**, *273*, 32730−32738.
(17) Farris, W.; Mansourian, S.; Chang, Y.; Lindsley, L.; Eckman, E. A.; Frosch, M. P.; Eckman, C. B.; Tanzi, R. E.; Selkoe, D. J.; Guenette, S. Insulin-degrading enzyme regulates the levels of insulin, amyloid beta-protein, and the beta-amyloid precursor protein intracellular domain *in vivo*. *Proc. Natl. Acad. Sci. U. S. A.* **2003**, *100*, 4162−4167.
(18) Sladek, R.; Rocheleau, G.; Rung, J.; Dina, C.; Shen, L.; Serre, D.; Boutin, P.; Vincent, D.; Belisle, A.; Hadjadj, S.; Balkau, B.; Heude, B.; Charpentier, G.; Hudson, T. J.; Montpetit, A.; Pshezhetsky, A. V.; Prentki, M.; Posner, B. I.; Balding, D. J.; Meyre, D.; Polychronakos, C.; Froguel, P. A genome-wide association study identifies novel risk loci for type 2 diabetes. *Nature* **2007**, *445*, 881−885.
(19) Steneberg, P.; Bernardo, L.; Edfalk, S.; Lundberg, L.; Backlund, F.; Ostenson, C. G.; Edlund, H. The type 2 diabetes-associated gene ide is required for insulin secretion and suppression of α-synuclein levels in β-cells. *Diabetes* **2013**, *62*, 2004−2014.
(20) Abdul-Hay, S. O.; Lane, A. L.; Caulfield, T. R.; Claussin, C.; Bertrand, J.; Masson, A.; Choudhry, S.; Fauq, A. H.; Maharvi, G. M.; Leissring, M. A. Optimization of peptide hydroxamate inhibitors of insulin-degrading enzyme reveals marked substrate-selectivity. *J. Med. Chem.* **2013**, *56*, 2246−2255.
(21) Maianti, J. P.; McFedries, A.; Foda, Z. H.; Kleiner, R. E.; Du, X. Q.; Leissring, M. A.; Tang, W. J.; Charron, M. J.; Seeliger, M. A.; Saghatelian, A.; Liu, D. R. Anti-diabetic activity of insulin-degrading enzyme inhibitors mediated by multiple hormones. *Nature* **2014**, *511*, 94−98.
(22) Campbell, J. E.; Drucker, D. J. Pharmacology, physiology, and mechanisms of incretin hormone action. *Cell Metab.* **2013**, *17*, 819−837.
(23) Thornberry, N. A.; Weber, A. E. Discovery of JANUVIA (Sitagliptin), a selective dipeptidyl peptidase IV inhibitor for the treatment of type 2 diabetes. *Curr. Top. Med. Chem.* **2007**, *7*, 557−568.
(24) Rachman, J.; Barrow, B. A.; Levy, J. C.; Turner, R. C. Near-normalisation of diurnal glucose concentrations by continuous administration of glucagon-like peptide-1 (GLP-1) in subjects with NIDDM. *Diabetologia* **1997**, *40*, 205−211.
(25) Kieffer, T. J.; Mcintosh, C. H.; Pederson, R. A. Degradation of glucose-dependent insulinotropic polypeptide and truncated glucagon-like peptide 1 *in vitro* and *in vivo* by dipeptidyl peptidase IV. *Endocrinology* **1995**, *136*, 3585−3596.
(26) Marguet, D.; Baggio, L.; Kobayashi, T.; Bernard, A. M.; Pierres, M.; Nielsen, P. F.; Ribel, U.; Watanabe, T.; Drucker, D. J.; Wagtmann, N. Enhanced insulin secretion and improved glucose tolerance in mice lacking CD26. *Proc. Natl. Acad. Sci. U. S. A.* **2000**, *97*, 6874−6879.
(27) Schafmeister, C. E.; Po, J.; Verdine, G. L. An all-hydrocarbon cross-linking system for enhancing the helicity and metabolic stability of peptides. *J. Am. Chem. Soc.* **2000**, *122*, 5891.
(28) Walensky, L. D.; Kung, A. L.; Escher, I.; Malia, T. J.; Barbuto, S.; Wright, R. D.; Wagner, G.; Verdine, G. L.; Korsmeyer, S. J. Activation of apoptosis *in vivo* by a hydrocarbon-stapled BH3 helix. *Science* **2004**, *305*, 1466−1470.
(29) Glas, A.; Bier, D.; Hahne, G.; Rademacher, C.; Ottmann, C.; Grossmann, T. N. Constrained peptides with target-adapted cross-links as inhibitors of a pathogenic protein-protein interaction. *Angew. Chem., Int. Ed.* **2014**, *53*, 2489−2493.
(30) Kruger, D. M.; Glas, A.; Bier, D.; Pospiech, N.; Wallraven, K.; Dietrich, L.; Ottmann, C.; Koch, O.; Hennig, S.; Grossmann, T. N. Structure-based design of non-natural macrocyclic peptides that inhibit protein-protein interactions. *J. Med. Chem.* **2017**, *60*, 8982−8988.
(31) Fremaux, J.; Mauran, L.; Pulka-Ziach, K.; Kauffmann, B.; Odaert, B.; Guichard, G. α-Peptide-oligourea chimeras: stabilization of short α-helices by non-peptide helical foldamers. *Angew. Chem., Int. Ed.* **2015**, *54*, 9816−9820.
(32) Wechsel, R.; Maury, J.; Fremaux, J.; France, S. P.; Guichard, G.; Clayden, J. Inducing achiral aliphatic oligoureas to fold into helical conformations. *Chem. Commun.* **2014**, *50*, 15006−15009.
(33) Hager, M. V.; Johnson, L. M.; Wootten, D.; Sexton, P. M.; Gellman, S. H. β-Arrestin-biased agonists of the GLP-1 receptor from β-amino acid residue incorporation into GLP-1 analogues. *J. Am. Chem. Soc.* **2016**, *138*, 14970−14979.
(34) Johnson, L. M.; Barrick, S.; Hager, M. V.; McFedries, A.; Homan, E. A.; Rabaglia, M. E.; Keller, M. P.; Attie, A. D.; Saghatelian, A.; Bisello, A. A potent alpha/beta-peptide analogue of GLP-1 with prolonged action *in vivo*. *J. Am. Chem. Soc.* **2014**, *136*, 12848−12851.
(35) Cui, H. K.; Guo, Y.; He, Y.; Wang, F. L.; Chang, H. N.; Wang, Y. J.; Wu, F. M.; Tian, C. L.; Liu, L. Diaminodiacid-based solid-phase synthesis of peptide disulfide bond mimics. *Angew. Chem., Int. Ed.* **2013**, *52*, 9558−9562.
(36) Cui, H. K.; Qing, J.; Guo, Y.; Wang, Y. J.; Cui, L. J.; He, T. H.; Zhang, L.; Liu, L. Stapled peptide-based membrane fusion inhibitors of hepatitis C virus. *Bioorg. Med. Chem.* **2013**, *21*, 3547−3554.
(37) Guo, Y.; Sun, D. M.; Wang, F. L.; He, Y.; Liu, L.; Tian, C. L. Diaminodiacid bridges to improve folding and tune the bioactivity of disulfide-rich peptides. *Angew. Chem., Int. Ed.* **2015**, *54*, 14276−14281.
(38) Kritzer, J. A. Grand challenge commentary: beyond discovery: probes that see, grab and poke. *Nat. Chem. Biol.* **2010**, *6*, 868−870.
(39) Blackwell, H. E.; Grubbs, R. H. Highly efficient synthesis of covalently cross-linked peptide helices by ring-closing metathesis. *Angew. Chem., Int. Ed.* **2010**, *37*, 3281−3284.
(40) Athanassiou, Z.; Dias, R. L.; Moehle, K.; Dobson, N.; Varani, G.; Robinson, J. A. Structural mimicry of retroviral tat proteins by constrained beta-hairpin peptidomimetics: ligands with high affinity and selectivity for viral TAR RNA regulatory elements. *J. Am. Chem. Soc.* **2004**, *126*, 6906−6913.
(41) Chatterjee, B.; Saha, I.; Raghothama, S.; Aravinda, S.; Rai, R.; Shamala, N.; Balaram, P. Designed peptides with homochiral and heterochiral diproline templates as conformational constraints. *Chem. - Eur. J.* **2008**, *14*, 6192−6204.
(42) Karle, I. L.; Awasthi, S. K.; Balaram, P. A designed beta-hairpin peptide in crystals. *Proc. Natl. Acad. Sci. U. S. A.* **1996**, *93*, 8189−8193.
(43) Haque, T. S.; Little, J. C.; Gellman, S. H. Mirror image″ reverse turns promote beta-hairpin formation. *J. Am. Chem. Soc.* **1994**, *116*, 4105−4106.
(44) Stanger, H. E.; Gellman, S. H. Rules for antiparallel β-sheet design: d-Pro-Gly is superior to l-Asn-Gly for β-hairpin nucleation1. *J. Am. Chem. Soc.* **1998**, *75*, 4236−4237.
(45) Masterson, L. R.; Etienne, M. A.; Porcelli, F.; Barany, G.; Hammer, R. P.; Veglia, G. Nonstereogenic alpha-aminoisobutyryl-glycyl dipeptidyl unit nucleates type I' beta-turn in linear peptides in aqueous solution. *Biopolymers* **2007**, *88*, 746−753.
(46) Aemissegger, A.; Kräutler, V.; van Gunsteren, W. F.; Hilvert, D. A photoinducible β-hairpin. *J. Am. Chem. Soc.* **2005**, *127*, 2929−2936.
(47) Diaz, H.; Espina, J. R.; Kelly, J. W. A dibenzofuran-based amino acid designed to nucleate antiparallel beta-sheet structure: evidence for intramolecular hydrogen-bond formation. *J. Am. Chem. Soc.* **1992**, *114*, 8316−8318.
(48) Tsang, K. Y.; Diaz, H.; Graciani, N.; Kelly, J. W. Hydrophobic cluster formation is necessary for dibenzofuran-based amino acids to function as beta-sheet nucleators. *J. Am. Chem. Soc.* **1994**, *116*, 3988−4005.
(49) Pelay-Gimeno, M.; Glas, A.; Koch, O.; Grossmann, T. N. Structure-based design of inhibitors of protein-protein interactions: mimicking peptide binding epitopes. *Angew. Chem., Int. Ed.* **2015**, *54*, 8896−8927.

DOI: 10.1021/acs.jmedchem.8b00418
J. Med. Chem. 2018, 61, 8174−8185

(50) Zhao, H.; Liu, Q. S.; Geng, H.; Tian, Y.; Cheng, M.; Jiang, Y. H.; Xie, M. S.; Niu, X. G.; Jiang, F.; Zhang, Y. O.; Lao, Y. Z.; Wu, Y. D.; Xu, N. H.; Li, Z. G. Crosslinked aspartic acids as helix-nucleating templates. *Angew. Chem., Int. Ed.* **2016**, *55*, 12088−12093.
(51) Fasan, R.; Dias, R. L.; Moehle, K.; Zerbe, O.; Vrijbloed, J. W.; Obrecht, D.; Robinson, J. A. Using a beta-hairpin to mimic an alpha-helix: cyclic peptidomimetic inhibitors of the p53-HDM2 protein-protein interaction. *Angew. Chem., Int. Ed.* **2004**, *43*, 2109−2112.
(52) Fadzen, C. M.; Wolfe, J. M.; Cho, C. F.; Chiocca, E. A.; Lawler, S. E.; Pentelute, B. L. Perfluoroarene-based peptide macrocycles to enhance penetration across the blood-brain barrier. *J. Am. Chem. Soc.* **2017**, *139*, 15628−15631.
(53) Spokoyny, A. M.; Zou, Y.; Ling, J. J.; Yu, H.; Lin, Y. S.; Pentelute, B. L. A perfluoroaryl-cysteine S(N)Ar chemistry approach to unprotected peptide stapling. *J. Am. Chem. Soc.* **2013**, *135*, 5946−5949.
(54) Maynard, S.; Almeida, A. M.; Yoshimi, Y.; Gellman, S. H. New charge-bearing amino acid residues that promote β-sheet secondary structure. *J. Am. Chem. Soc.* **2014**, *136*, 16683−16688.
(55) Brandts, J. F.; Halvorson, H. R.; Brennan, M. Consideration of the possibility that the slow step in protein denaturation reactions is due to cis-trans isomerism of proline residues. *Biochemistry* **1975**, *14*, 4953−4963.
(56) Späth, J.; Stuart, F.; Jiang, L.; Robinson, J. A. Stabilization of a β-hairpin conformation in a cyclic peptide using the templating effect of a heterochiral diproline unit. *Helv. Chim. Acta* **1998**, *81*, 1726−1738.
(57) Vijayakumar, A.; Aryal, P.; Wen, J.; Syed, I.; Vazirani, R. P.; Moraes-Vieira, P. M.; Camporez, J. P.; Gallop, M. R.; Perry, R. J.; Peroni, O. D.; Shulman, G. I.; Saghatelian, A.; McGraw, T. E.; Kahn, B. B. Absence of carbohydrate response element binding protein in adipocytes causes systemic insulin resistance and impairs glucose transport. *Cell Rep.* **2017**, *21*, 1021−1035.
(58) Oller-Salvia, B.; Sánchez-Navarro, M.; Ciudad, S.; Guiu, M.; Arranz-Gibert, P.; Garcia, C.; Gomis, R. R.; Cecchelli, R.; García, J.; Giralt, E.; Teixido, M. MiniAp-4: a venom-inspired peptidomimetic for brain delivery. *Angew. Chem., Int. Ed.* **2016**, *55*, 572−575.
(59) Wang, D.; Chen, K.; Kulp, J. L., Iii; Arora, P. S. Evaluation of biologically relevant short alpha-helices stabilized by a main-chain hydrogen-bond surrogate. *J. Am. Chem. Soc.* **2006**, *128*, 9248−9256.
(60) Vaz, B.; Mocklinghoff, S.; Folkertsma, S.; Lusher, S.; de Vlieg, J.; Brunsveld, L. Computational design, synthesis, and evaluation of miniproteins as androgen receptor coactivator mimics. *Chem. Commun.* **2009**, *0*, 5377−5379.
(61) Zhao, B.; Yang, D.; Wong, J. H.; Wang, J.; Yin, C.; Zhu, Y.; Fan, S.; Ng, T. B.; Xia, J.; Li, Z. A thioether-stabilized d-proline-l-proline-induced beta-hairpin peptide of defensin segment increases its anti-candida albicans ability. *ChemBioChem* **2016**, *17*, 1416−1420.
(62) Liu, Y.; Xia, X.; Xu, L.; Wang, Y. Design of hybrid beta-hairpin peptides with enhanced cell specificity and potent anti-inflammatory activity. *Biomaterials* **2013**, *34*, 237−250.
(63) Yin, F.; Hu, K.; Chen, S.; Wang, D.; Zhang, J.; Xie, M.; Yang, D.; Qiu, M.; Zhang, H.; Li, Z. Black phosphorus quantum dot based novel siRNA delivery systems in human pluripotent teratoma PA-1 cells. *J. Mater. Chem. B* **2017**, *5*, 5433−5440.
(64) Choi, E. K.; Rajasekaran, M.; Sul, O. J.; Joe, Y.; Chung, H. T.; Yu, R.; Choi, H. S. Impaired insulin signaling upon loss of ovarian function is associated with a reduction of tristetraprolin and an increased stabilization of chemokine in adipose tissue. *Mol. Cell. Endocrinol.* **2018**, *461*, 122−131.
(65) Luo, G.; Kong, X.; Lu, L.; Xu, X.; Wang, H.; Ma, X. Glucagon-like peptide 1 potentiates glucotoxicity-diminished insulin secretion via stimulation of cAMP-PKA signaling in INS-1E cells and mouse islets. *Int. J. Biochem. Cell Biol.* **2013**, *45*, 483−490.
(66) Liu, L. Z.; Cheung, S. C. K.; Lan, L. L.; Ho, S. K. S.; Chan, J. C. N.; Tong, P. C. Y. Microtubule network is required for insulin-induced signal transduction and actin remodeling. *Mol. Cell. Endocrinol.* **2013**, *365*, 64−74.
(67) Liu, L. Z.; Cheung, S. C. K.; Lan, L. L.; Ho, S. K. S.; Xu, H. X.; Chan, J. C. N.; Tong, P. C. Y. Berberine modulates insulin signaling transduction in insulin-resistant cells. *Mol. Cell. Endocrinol.* **2010**, *317*, 148−153.
(68) Tian, Y.; Zeng, X.; Li, J.; Jiang, Y.; Zhao, H.; Wang, D.; Huang, X.; Li, Z. Achieving enhanced cell penetration of short conformationally constrained peptides through amphiphilicity tuning. *Chem. Sci.* **2017**, *8*, 7576−7581.
(69) Li, W.; Ma, L.; Yang, G.; Gan, W. B. REM sleep selectively prunes and maintains new synapses in development and learning. *Nat. Neurosci.* **2017**, *20*, 427−437.
(70) Yang, L.; Lu, Y.; Qi, J.; Nie, S.; Hu, F.; Pan, W.; Wu, W. Solid self-nanoemulsifying cyclosporin A pellets prepared by fluid-bed coating: preparation, characterization and *in vitro* redispersibility. *Int. J. Nanomed.* **2013**, *6*, 795−805.

DOI: 10.1021/acs.jmedchem.8b00418
J. Med. Chem. 2018, 61, 8174−8185